

Energy spectra of three electrons in SiGe/Si/SiGe laterally coupled triple quantum dots

Y. F. Ren, L. Wang,* Z. Liu, and M. W. Wu†

*Hefei National Laboratory for Physical Sciences at Microscale and Department of Physics,
University of Science and Technology of China, Hefei, Anhui, 230026, China*

(Dated: September 7, 2021)

We investigate the energy spectra of three electrons in SiGe/Si/SiGe equilateral triangular and symmetric linear triple quantum dots in the presence of magnetic (in either Faraday or Voigt configuration) and electric fields with single valley approximation by using the real-space configuration interaction method. The strong electron-electron Coulomb interaction, which is crucial to the energy spectra, is explicitly calculated whereas the weak spin-orbit coupling is treated perturbatively. In both equilateral triangular and symmetric linear triple quantum dots, we find doublet-quartet transition of ground-state spin configuration by varying dot size or interdot distance in the absence of external fields. This transition has not been reported in the literature on triple quantum dots. In the magnetic-field (Faraday configuration) dependence of energy spectra, we find anticrossings with large energy splittings between the energy levels with the same spin state in the absence of the spin-orbit coupling. This anticrossing behavior originates from the triple quantum dot confinement potential. In addition, with the inclusion of the spin-orbit coupling, we find that all the intersections shown in the equilateral triangular case become anticrossing whereas only part of the intersections in symmetric linear case show anticrossing behavior in the presence of magnetic field in either the Faraday or Voigt configuration. All the anticrossing behaviors are analyzed based on symmetry consideration. Moreover, we show that the electric field can effectively influence the energy levels and the charge configurations.

PACS numbers: 73.21.La, 73.22.-f, 61.72.uf, 71.70.Ej

I. INTRODUCTION

Spin-based qubits in semiconductor quantum dots (QDs) have been widely investigated for promising applications in quantum information processing.¹⁻⁶ So far, much attention has been paid to spin qubits utilizing single-electron Zeeman sublevels and two-electron singlet-triplet states in both single and double QDs.^{1-4,7-30} Similar to the proposals in single and double QDs, three-electron doublet states in linear triple QDs³¹⁻³⁴ (TQDs) or chirality states in triangular TQDs^{35,36} have also been raised to realize spin qubits recently. Additionally, based on Zeeman sublevels of single electron in each QD as a spin qubit, TQDs can be used as a small circuit for constructing the QD network.^{5,37-41} This circuit has some intriguing functionalities. Specifically, it can be used to realize quantum teleportation without losing information.³⁸ Moreover, the entangled Greenberger-Horne-Zeilinger state and Werner state in this system can be applied for quantum error correction.^{39,40} All these potential applications may make TQDs attractive for quantum computation.

Recently, electronic and spin properties of TQDs with few electrons have been studied both experimentally and theoretically.^{5,42-58} In experiments, the stability diagrams of linear Si TQDs^{43,46,48} and both linear^{42,44,45} and triangular⁴⁷ GaAs TQDs have been measured. In addition, the coherent manipulation of doublet-quartet⁴⁹ or doublet-doublet⁵⁰ states in GaAs linear TQDs has been realized very recently. Theoretically, both energy spec-

tra and spin configurations of the lowest several states of few electrons in TQDs have been investigated.⁵¹⁻⁵⁸ Korkusinsik *et al.*⁵⁴ proposed a set of topological Hund's rules to understand the spin configurations of the ground states of few electrons in GaAs TQDs in the absence of external fields. Delgado *et al.*⁵⁶ showed the transition of the spin configurations of few-electron states in GaAs TQDs by tuning the perpendicular magnetic field (i.e., the Faraday configuration). Bulka *et al.*⁵⁷ investigated both the linear and nonlinear Stark effects induced by the in-plane electric field. In addition to these works on triangular TQDs, Hsieh *et al.*⁵⁸ also studied the dependence of the energy spectra on detuning energy in linear GaAs TQDs. It is noted that all the above works are based on the Hubbard model. Utilizing this model, the electron-electron Coulomb interaction, which is crucial to the energy spectra,^{16,22,28,29,59} is not explicitly included, but rather given as Hubbard parameters. With the electron-electron Coulomb interaction explicitly calculated by using the real-space configuration interaction method, Hawrylak and Korkusinsik⁵² investigated the gate-voltage dependence of the three-electron energy spectra in triangular GaAs TQDs. However, the effects of the magnetic field and spin-orbit coupling (SOC), which have been shown to be very important to the energy spectra, were not studied in their work.^{16,22,29,59} It is further noted that most of the theoretical works on electronic and spin properties of few electrons in TQDs have focused on GaAs until now. As reported, the spin decoherence, which is essential for applications in quantum computation, is limited by the hyperfine interaction¹¹ and

spin-orbit coupling (SOC)^{60,61} in GaAs. In contrast to GaAs, Si has much better spin decoherence properties, which may make it more attractive.^{12,62–66} However, to the best of our knowledge, theoretical work specific to Si TQDs has not been reported.

In the present work, we investigate the energy spectra of three electrons in both equilateral triangular and symmetric linear Si TQDs in the presence of external magnetic and electric fields. The strong electron-electron Coulomb interaction is explicitly included by the real-space configuration interaction method whereas the SOC with much smaller energy is treated perturbatively. We first investigate the case of equilateral triangular TQDs where the dependences of energy spectra on the external either perpendicular magnetic or parallel magnetic (i.e., the Voigt configuration) field, dot size, interdot distance, and electric field are calculated. We find anticrossings with large energy splittings between the energy levels with the same spin state in the perpendicular magnetic-field dependence of the energy spectra in the absence of the SOC. These anticrossings, which have not been reported in the literature, originate from the equilateral triangular TQD confinement potential. As for the parallel magnetic-field dependence, the energy spectra only vary linearly due to the negligible orbital effect of the parallel magnetic field. In addition, we find doublet-quartet transition of the ground-state spin configuration by tuning the interdot distance or dot size in the absence of external fields and the SOC. We also find that the three-electron energy levels and their charge configurations can be strongly affected by the in-plane electric field. Then we turn to the case of symmetric linear TQDs where the effects of dot size, interdot distance, magnetic and electric fields on energy spectra are discussed. Anticrossings between the energy levels with the same spin state are observed in the perpendicular magnetic-field dependence of the energy spectra, which is similar to the case of the equilateral triangular TQDs. It is noted that with the inclusion of the SOC, all the intersections show anticrossing behavior in equilateral triangular TQD case whereas only part of them become anticrossing in symmetric linear TQD case.

This paper is organized as follows. In Sec. II, we introduce the model and lay out the formalism. Our main results are presented in Sec. III where the equilateral triangular and symmetric linear TQDs are investigated in Sec. IIIA and Sec. IIIB, respectively. We summarize in Sec. IV.

II. MODEL AND FORMALISM

We set up our model in a SiGe/Si/SiGe quantum well grown along [001] direction (the z -axis). A strong confinement along this direction splits the six-fold degenerate conduction band minima or valleys of bulk Si into a four-fold degeneracy and a two-fold one with a large energy splitting.^{67,68} The two-fold degenerate valleys with

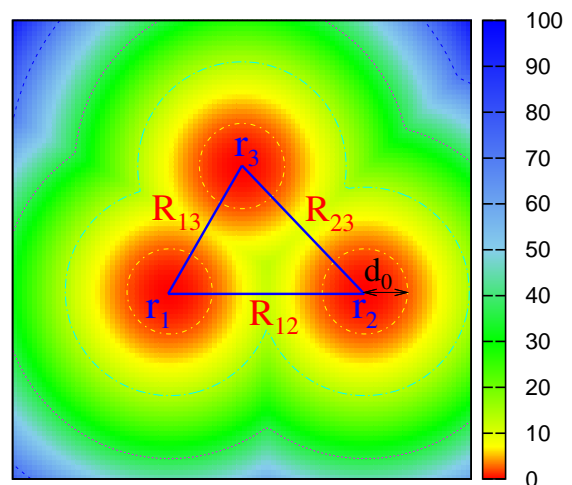


FIG. 1: (Color online) Schematic of the laterally coupled TQD potential. \mathbf{r}_i ($i = 1-3$) is the location of dot i . d_0 and R_{ij} represent the effective dot size and interdot distance between dots i and j , respectively. It is noted that three dots have same effective dot size.

lower energy can be further lifted by a valley splitting in the presence of interface scattering.^{65,68–70} Here, we focus on a large valley splitting case where only the lowest valley eigenstate is relevant.^{21,30} Furthermore, we restrict the system to a two-dimensional one by considering that the confinement along the z -axis is much stronger than the lateral ones.^{30,65} The lateral confinement potential is chosen as $V_c(\mathbf{r}) = \frac{1}{2}m_t\omega_0^2\min\{(\mathbf{r} - \mathbf{r}_1)^2, (\mathbf{r} - \mathbf{r}_2)^2, (\mathbf{r} - \mathbf{r}_3)^2\}$, where m_t and ω_0 represent the in-plane effective mass and confining potential frequency, respectively.^{71,72} A schematic of TQDs is shown in Fig. 1 where three QDs are located at \mathbf{r}_i ($i = 1-3$) with the effective dot size and the interdot distance between dots i and j being $d_0 = \sqrt{\hbar\pi/(m_t\omega_0)}$ and $R_{ij} = |\mathbf{r}_i - \mathbf{r}_j|$, respectively. The TQD confinement potential can be tuned by both the dot size and interdot distance. In the present work, we focus on equilateral triangular and symmetric linear TQDs with the interdot distances being $R_{12} = R_{23} = R_{13} = x_0$ and $R_{13} = R_{23} = R_{12}/2 = x_0/2$, respectively. In our calculation, we set the origin to be $(\mathbf{r}_1 + \mathbf{r}_2)/2$ and the x -axis along the direction $\mathbf{r}_2 - \mathbf{r}_1$, thus $\mathbf{r}_{1,2} = (\mp x_0/2, 0)$, $\mathbf{r}_3 = (0, \sqrt{3}x_0/2)$ and $(0, 0)$ for equilateral triangular and symmetric linear TQDs, respectively.

In the presence of external magnetic field $\mathbf{B} = B_\perp \hat{\mathbf{z}} + B_\parallel \hat{\mathbf{x}}$, the single-electron Hamiltonian reads²⁹

$$H_e = \frac{P_x^2 + P_y^2}{2m_t} + V_c(\mathbf{r}) + H_{\text{so}}(\mathbf{P}) + H_Z + H_E, \quad (1)$$

where $\mathbf{P} = \mathbf{p} + (e/c)\mathbf{A} = -i\hbar\nabla + (e/c)\mathbf{A}$ with $\mathbf{A} = (-y, x)B_\perp/2$. It is noted that the orbital effect of the in-plane magnetic field is neglected due to a strong confinement along the z -axis.¹⁶ $H_{\text{so}}(\mathbf{P})$ represents the SOC Hamiltonian including both the Rashba term⁶¹ due to

the structure inversion asymmetry and the interface-inversion asymmetry (IIA) term.⁶⁴ Then it can be given by

$$H_{\text{so}}(\mathbf{P}) = a_0(P_x\sigma_y - P_y\sigma_x) + b_0(-P_x\sigma_x + P_y\sigma_y), \quad (2)$$

with $\sigma_{x(y)}$, a_0 and b_0 representing the Pauli matrix, strengths of the Rashba and IIA terms, respectively. $H_Z = g\mu_B(B_\perp\sigma_z + B_\parallel\sigma_x)/2$ is the Zeeman term where g , μ_B , and σ_z stand for the Landé factor,⁷³ Bohr magneton,⁷⁴ and Pauli matrix, separately. $H_E = eEx$ represents the electric field term with an electric field applied along the x -direction.

To obtain a complete set of the single-electron orbital basis functions, which will be used to construct the three-electron ones, we define $H_0 = (P_x^2 + P_y^2)/(2m_t) + V_c(\mathbf{r}) + H_E$. Due to the complex TQD confinement potential $V_c(\mathbf{r})$, it is difficult to solve the Schrödinger equation of H_0 analytically. Hence, we calculate the eigenvalues and eigenstates of H_0 numerically by employing the finite difference method according to the report by Stano and Fabian.⁷⁵

For three-electron case, the total Hamiltonian can be expressed as

$$H_{\text{tot}} = H_e^1 + H_e^2 + H_e^3 + H_C^{12} + H_C^{23} + H_C^{13}. \quad (3)$$

Here, H_e^i ($i = 1-3$) represents the single-electron Hamiltonian of the i th electron given by Eq. (1). H_C^{ij} stands for the Coulomb interaction between the i th and j th electrons, which is given by

$$H_C^{ij} = \frac{e^2}{4\pi\epsilon_0\kappa|\mathbf{r}_i - \mathbf{r}_j|}, \quad (4)$$

with ϵ_0 and κ being the vacuum dielectric constant and relative static dielectric constant,⁷⁶ separately.

According to the approach widely used in the nuclear physics when building up the wavefunction of baryons composed of three quarks with total spin being 1/2 for each quark,^{77,78} we construct the three-electron basis functions as follows. These three-electron basis functions are composed of both spin and orbital parts. We first construct the spin part in the form of either quartet or doublet⁷⁹ by Clebsch-Gordan coefficient method.⁸⁰ It is noted that the quartet spin wavefunctions are exchange symmetric whereas the doublet spin wavefunctions are of mixed symmetry.⁸¹ With these spin states, we then build up the corresponding orbital wavefunctions to make the total three-electron basis functions exchange antisymmetric for any two electrons. The detailed expressions of three-electron total basis functions can be found in Ref. 59. These total basis functions are still denoted by either quartet or doublet states according to their spin states.

After obtaining these three-electron basis functions, one can calculate the matrix elements of three-electron Hamiltonian H_{tot} [see Eq. (3)] including the orbital energy, Zeeman splitting, SOC and Coulomb interaction.⁸²

Since the matrix elements of the SOC is about three orders of magnitude smaller than others, we first calculate the three-electron eigenvalues and eigenstates by exactly diagonalizing the three-electron Hamiltonian matrix in the absence of SOC. Then based on the obtained three-electron eigenvalues and eigenstates, we include the SOC perturbatively.

III. NUMERICAL RESULTS

In our calculation, the effective mass $m_t = 0.19m_0$ with m_0 being the free electron mass.⁸³ The strengths of the SOC are chosen as $a_0 = -6.06$ m/s and $b_0 = -30.31$ m/s corresponding to the electric field along the growth direction being 30 kV/cm.⁶⁴ The Landé factor $g = 2$ (Ref. 73) and the relative dielectric constant $\kappa = 11.9$.⁷⁶ The grid points used to diagonalize the single-electron Hamiltonian are 95×95 with the accuracy of the energy being around 10^{-5} meV. Based on these single-electron wavefunctions, the lowest 11194 doublet and 10128 quartet basis functions are taken to obtain convergent three-electron energy spectra and eigenstates with the exact-diagonalization method. The energy precision is also around 10^{-5} meV.

A. Equilateral triangular TQDs

In this part, we focus on the case of equilateral triangular TQDs. We first study both the perpendicular and parallel magnetic-field dependences of three-electron energy spectra where detailed discussions about anticrossing behavior induced by the equilateral triangular TQD confinement potential and the SOC are presented. We then investigate the doublet-quartet transition of ground-state spin configuration by tuning the interdot distance or the dot size in the absence of external fields and the SOC. In addition, the electric-field dependence of energy levels and their charge configurations are also shown.

1. Anticrossings in the magnetic-field dependence of three-electron energy spectra

We first investigate the perpendicular magnetic-field dependence of energy spectra in the absence of the SOC. In Fig. 2(a), we plot the magnetic-field dependence of the lowest few energy levels with the interdot distance x_0 being 11.6 nm and dot size d_0 being 29 nm. These energy levels are denoted as either $D_{\pm 1/2}$ or $Q_{\pm 1/2, \pm 3/2}$ according to their spin states. We find that, in the absence of the magnetic field, the ground state is four-fold degenerate quartet and the lowest doublet state is also four-fold degenerate as shown in the left inset in Fig. 2(a). With the magnetic field applied, the degeneracy of these states is lifted due to the orbital effect of the magnetic field and the Zeeman splitting, leading to many intersections.⁵⁹

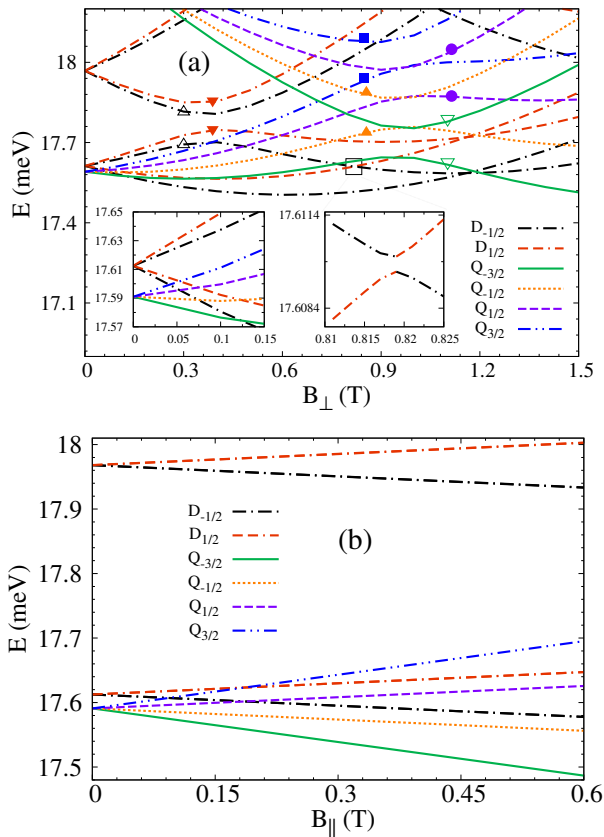


FIG. 2: (Color online) (a) The lowest several energy levels *vs.* the perpendicular magnetic field B_{\perp} in equilateral triangular TQDs. The energy levels related to six anticrossings with large energy splittings are labelled by symbols \blacktriangledown , \triangle , \bullet , \blacktriangle , \blacksquare and ∇ . The left inset enlarges the energy spectra in the vicinity of $B_{\perp} \sim 0$ T whereas the right inset zooms one anticrossing induced by the SOC in the vicinity of $B_{\perp} \sim 0.819$ T. (b) The lowest several energy levels *vs.* parallel magnetic field along the x -direction. Here, $d_0 = 29$ nm and $x_0 = 11.6$ nm.

This is similar to the case of three electrons in single Si QDs.⁵⁹ In contrast to the single QD case, we find six anticrossings with large energy splittings between the energy levels with the same spin state in Fig. 2(a). Specifically, at $B_{\perp} = 0.4$ T, we find two anticrossings with energy splitting about 0.105 meV between two $D_{1/2}$ ($D_{-1/2}$) states labelled by \blacktriangledown (\triangle). At $B_{\perp} = 1$ T, four anticrossings with energy splitting about 0.102 meV are between the lowest two states of Q_{S_z} with S_z being $\pm 1/2$ and $\pm 3/2$ labelled by \bullet , \blacktriangle , \blacksquare and ∇ , respectively. It is noted that this anticrossing behavior has not been reported in the literature on TQDs.

The underlying physics of these anticrossings can be understood as follows. It is noted that, in the absence of the SOC, the total spin S_{tot} and its z -component S_z are good quantum numbers. Therefore, the Hilbert space can be divided into independent subspaces according to S_{tot} and S_z and then we restrict to one subspace

in the following. For an infinitesimal interdot distance, i.e., $x_0 = 0$ nm, the equilateral triangular TQD confinement potential reduces to the limit of single QD one. Due to the rotation symmetry of the single QD case, the total azimuthal angular momentum L is also a good quantum number. We plot the perpendicular magnetic-field dependence of the lowest few energy levels with the corresponding L labelled in Fig. 6 in Appendix A. We find that there arise many intersections between the energy levels with the same spin state but with different L , which are just simple crossings. With the increase of interdot distance, the single QD confinement potential turns to the TQD one. The TQD confinement potential deviates from the single QD one and breaks the rotation symmetry, which indicates that L is no longer a good quantum number in TQDs. Specifically, in our case with equilateral triangular TQDs, the system has C_3 symmetry instead.⁸⁴ As a result, the subspace denoted by S_{tot} and S_z can be divided into three independent parts spanned by three-electron eigenstates in single QDs with $\{L|L = 3m + \chi\}$ (m integral, $\chi = 0, \pm 1$), respectively. It is noted that in each part, the eigenstates of three electrons in single QDs can be coupled with each other by the equilateral triangular TQD confinement potential. This coupling can make the intersections between the states in the same part in single QD case become anticrossing in TQD case as shown at $B_{\perp} = 0.4$ and 1 T in Fig. 2(a).

With the inclusion of the SOC, the three-electron energy spectra including the large energy splittings of the above anticrossings are almost unchanged. However, all the intersections mentioned previously become anticrossing with small energy splittings. One of these anticrossings (marked by open square at $B_{\perp} = 0.819$ T) is enlarged as shown in the right inset in Fig. 2(a) where the energy splitting is about 0.49 μeV . This anticrossing behavior originates from the effect of the SOC with the details shown in Appendix A.

We then turn to study the effect of the parallel magnetic field applied along the x -direction. In the absence of the SOC, the lowest several energy levels as function of the magnetic field are shown in Fig. 2(b) with the same dot size and interdot distance as the case of perpendicular magnetic field in Fig. 2(a). These energy levels are denoted by either $D_{\pm 1/2}$ or $Q_{\pm 1/2, \pm 3/2}$ according to the spin quantum numbers S_{tot} and its x -component S_x . We find that in contrast to the complex perpendicular magnetic-field dependence of energy spectra shown in Fig. 2(a), the energy levels show a simple linear dependence on the parallel magnetic field here. This can be understood that the parallel magnetic field affects the energy spectra only through the Zeeman splitting whereas the orbital effect is negligible owing to the strong confinement along the growth direction. Specifically, for $D_{\pm 1/2}$ ($Q_{\pm 1/2, \pm 3/2}$), the x -components of the total spins are $\pm 1/2$ ($\pm 1/2, \pm 3/2$), which indicate that these energy levels change linearly with the parallel magnetic field. This leads to the absence of the intersections between the energy levels with the same spin state and there-

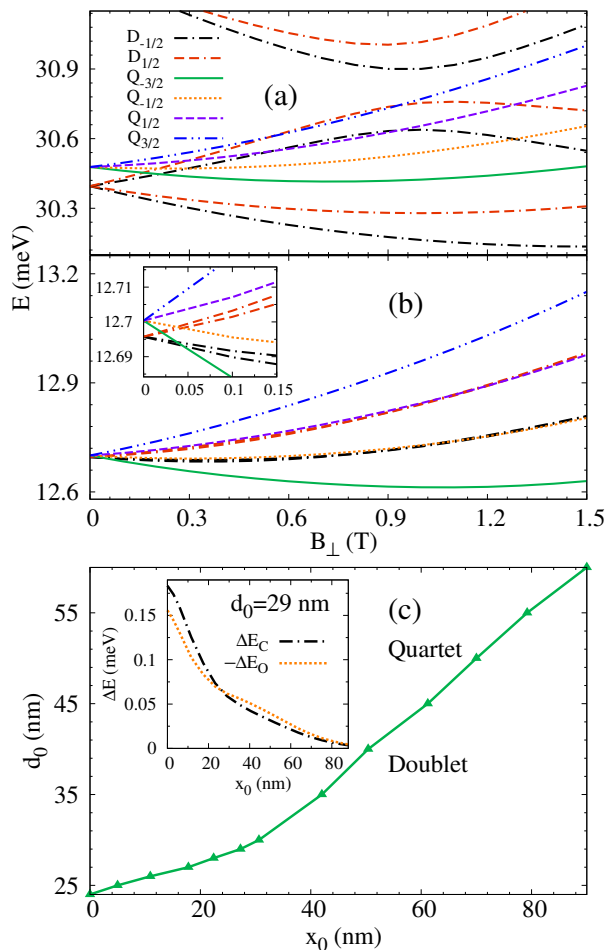


FIG. 3: (Color online) The lowest few energy levels *vs.* perpendicular magnetic field B_{\perp} in equilateral triangular TQDs with (a) $d_0 = 20$ nm, $x_0 = 11.6$ nm and (b) $d_0 = 29$ nm, $x_0 = 58.0$ nm. The inset in (b) enlarges the energy spectra in the vicinity of $B_{\perp} \sim 0$ T. (c) Spin configuration of the ground state *vs.* dot size and interdot distance in the absence of external fields with the green solid curve with symbol \blacktriangle representing the crossover between different spin configurations “Quartet” and “Doublet”. In the inset, we also show the interdot-distance dependence of the Coulomb energy difference ΔE_C (black chain) and orbital energy differences $-\Delta E_O$ (yellow dotted) between the lowest doublet and quartet states. $d_0 = 29$ nm.

fore the anticrossings between these states are absent. This is very different from the case of the perpendicular magnetic field. In addition, similar to the perpendicular magnetic field case, we also find that all the intersections shown in Fig. 2(b) become anticrossing with the inclusion of the SOC.

2. Doublet-quartet transition of ground-state spin configuration

In addition to the anticrossing behavior, we also study the transition of ground-state spin configuration in the absence of the external fields and the SOC. It is noted that the ground state is quartet at zero magnetic field as shown in the left inset in Fig. 2 when $d_0 = 29$ nm and $x_0 = 11.6$ nm. This spin configuration of the ground state in the absence of external fields has not been reported in the literature on TQDs. By varying either the dot size ($d_0 = 20$ nm, $x_0 = 11.6$ nm) or interdot distance ($d_0 = 29$ nm, $x_0 = 58.0$ nm), we find that the ground-state spin configurations become doublet instead at $B_{\perp} = 0$ T as shown in Figs. 3(a) and (b), respectively. Therefore, the doublet-quartet transition of ground-state spin configuration can be realized by tuning either the dot size or the interdot distance. Furthermore, to show the spin configuration of ground state as function of the dot size and the interdot distance, we plot a phase-diagram-like picture in Fig. 3(c) by calculating the energy difference ΔE_{DQ} between the lowest doublet (E_D) and quartet (E_Q) states (i.e., $\Delta E_{DQ} = E_D - E_Q$). In this figure, the doublet and quartet ground-state spin configurations are separated by a solid curve with \blacktriangle corresponding to $\Delta E_{DQ} = 0$. Specifically, as the dot size decreases, the ground-state spin configuration changes from quartet to doublet, which is similar to the case in single QDs reported by Liu *et al.*⁵⁹

As for the effect of interdot distance x_0 , we also find a transition of the spin configuration of ground state from quartet to doublet as x_0 increases. This can be understood as follows. It is noted that the energy difference between the lowest doublet and quartet states ΔE_{DQ} is contributed by the orbital energy difference ΔE_O and Coulomb energy difference ΔE_C , i.e., $\Delta E_{DQ} = \Delta E_C + \Delta E_O$. With a specific dot size d_0 being 29 nm, we calculate the interdot-distance dependence of ΔE_C and $-\Delta E_O$ as shown in Fig. 3(c). We find that both ΔE_C and $-\Delta E_O$ decrease with the increase of interdot distance. However, ΔE_C decreases faster than $-\Delta E_O$ and an intersection (i.e., $\Delta E_{DQ} = 0$) occurs at $x_0 \sim 26$ nm, indicating a transition of ground-state spin configuration from quartet to doublet. This is similar to the case of double QDs where the transition of ground-state spin configuration can also be realized by tuning the interdot distance.²⁹

3. Electric-field dependence of energy spectra and charge configurations

We also investigate the dependence of the lowest several energy levels on the electric field along x -direction in the absence of the SOC and magnetic field. We first focus on the ground state as shown in Fig. 4(a) which is two-fold degenerate doublet. We find that the ground-state energy changes slowly in small electric field regime

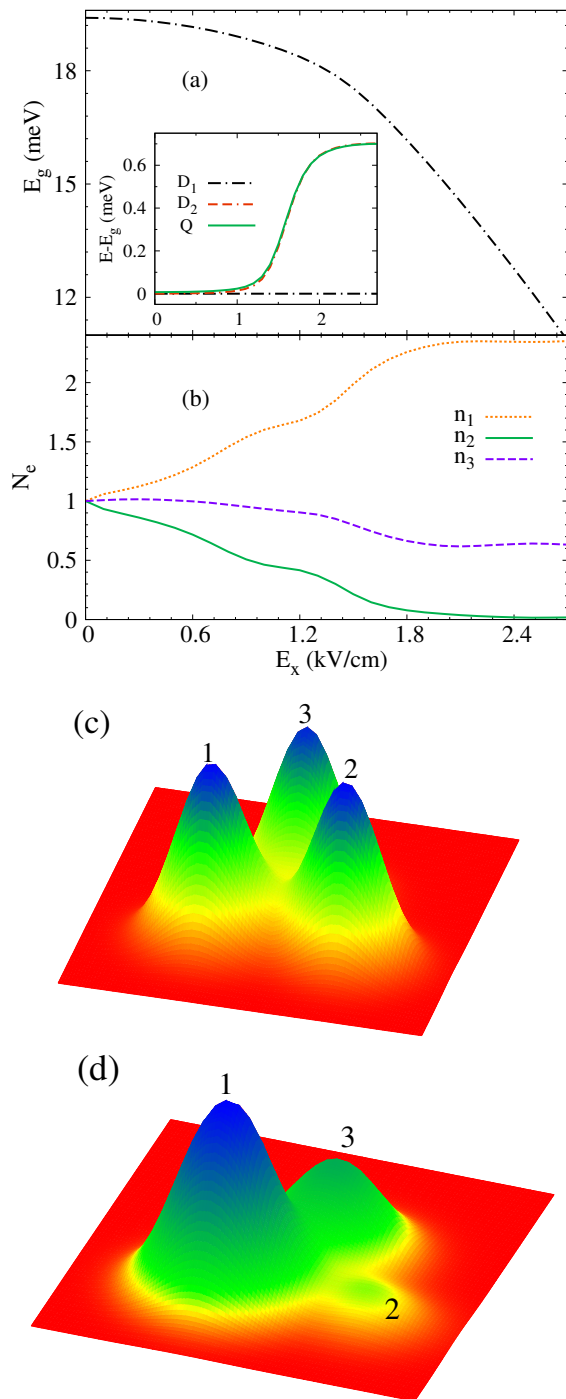


FIG. 4: (Color online) (a) Energy of the ground state E_g vs. electric field applied along the x -direction E_x . The lowest several energy levels with the energy of the ground state subtracted are shown in the inset. D_1 and D_2 are two-fold degenerate doublet states whereas Q represents the lowest four-fold degenerate quartet states. (b) Charge configuration (n_1, n_2, n_3) of ground state vs. E_x . (c) and (d) show the charge density distributions of three electrons in the ground states with $(1, 1, 1)$ and $(2, 0, 1)$ configurations, respectively. Here, $d_0 = 20$ nm and $x_0 = 58$ nm.

whereas it decreases rapidly when the electric field becomes strong. This can be understood from the variation of charge configuration of the ground state. As shown in Fig. 4(b), the charge configuration is denoted by (n_1, n_2, n_3) with n_i ($i = 1-3$) representing the electron occupation number of the i th QD.⁸⁵ It is seen that, in small electric field regime, the charge configuration is close to $(1, 1, 1)$, whereas it changes to the configuration close to $(2, 0, 1)$ when the electric field is strong. The charge density distribution of three electrons in $(1, 1, 1)$ and $(2, 0, 1)$ configurations are plotted in Figs. 4(c) and (d), respectively. It is noted that the electric field term is given by $H_E = eEx$ according to Eq. (1). As a result, the variation of the single-electron energy in the middle QD (i.e., dot 3) is negligible since dot 3 is located at $x = 0$. In contrast, the single-electron energy in the right QD (i.e., dot 2) is raised whereas that in the left QD (i.e., dot 1) is suppressed due to the applied electric field. Therefore, close to $(1, 1, 1)$ configuration, i.e., the small electric field regime, the net contribution of the electric field is relatively small and thus the energy changes slowly with the increase of the electric field. When the electric field becomes strong, i.e., close to $(2, 0, 1)$ configuration, the energy due to the electric field decreases with increasing electric field whereas the contribution of the Coulomb energy presents an opposite trend. It is noted that the variation of the energy induced by the electric field is much larger than that of the Coulomb energy, which leads to a rapid decrease of the ground-state energy with the increase of the electric field.

Then we turn to the lowest several excited states. The dependence of these energy levels on the electric field is plotted in the inset in Fig. 4(a). In this figure, the energy levels are shown with the energy of the ground state subtracted to make them distinguishable. It is noted that the excited doublet state is two-fold degenerate whereas the excited quartet state is four-fold. Moreover, the behavior of the charge configurations of these states as function of the electric field is similar to that of the ground state.

B. Symmetric linear TQDs

In this part, we investigate the case of symmetric linear TQDs where the perpendicular magnetic-field dependence of the lowest several energy levels with $x_0/2 = 11.6$ nm and $d_0 = 29$ nm in the absence of the SOC are shown in Fig. 5. These energy levels are still denoted as either $D_{\pm 1/2}$ or $Q_{\pm 1/2, \pm 3/2}$ according to their spin states. It is seen that, as the magnetic field increases, there arise many intersections due to the Zeeman splitting and the orbital effect of the magnetic field, which is similar to the equilateral triangular TQD case. Additionally, at $B_{\perp} = 2.2$ T, one also observes an anticrossing between the lowest two states of $D_{-1/2}$ labelled by Δ . The underlying physics can be understood similar to the case of the equilateral triangular TQDs. We also focus on a specific subspace denoted by S_{tot} and S_z . This sub-

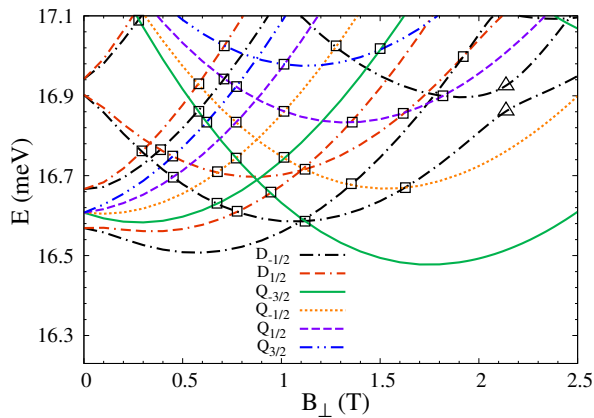


FIG. 5: (Color online) The lowest several energy levels *vs.* the perpendicular magnetic field B_{\perp} in symmetric linear TQDs. The energy levels related to the anticrossing with large energy splitting are labelled by \triangle . Open squares denote the intersections which become anticrossing due to the SOC. $d_0 = 29$ nm and $x_0/2 = 11.6$ nm.

space can be further divided into two independent parts since the system with the symmetric linear TQD confinement potential has C_2 symmetry.⁸⁴ These two parts are spanned by the three-electron eigenstates in single QDs with $\{L|L = 2m + \chi\}$ (m integral, $\chi = 0, 1$), respectively. The intersection between the energy levels in the same part in single QDs is lifted to show anticrossing behavior in symmetric linear TQD case as shown at $B_{\perp} = 2.2$ T. Moreover, we also find that only part of intersections show anticrossing behavior with the inclusion of the SOC, which are labelled by open squares in Fig. 5. The details are shown in Appendix A. This is different from the equilateral triangular TQD case where all the intersections become anticrossing.

In addition, compared with the equilateral triangular TQD case, similar behaviors such as the doublet-quartet transition of ground-state spin configuration by varying the dot size or interdot distance in the absence of the magnetic field and the SOC, variation of three-electron charge configuration by the electric field, and the linear dependence of energy spectra on parallel magnetic field can also be observed in symmetric linear TQDs.

IV. SUMMARY

In summary, we have investigated the three-electron energy spectra in laterally coupled SiGe/Si/SiGe TQDs with single valley approximation by utilizing the real-space configuration interaction method. The electron-electron Coulomb interaction, which is crucial to the energy spectra, is explicitly included whereas the relatively small SOC is treated perturbatively. The dependences of the energy spectra on the dot size, interdot distance, (either perpendicular or parallel) magnetic field, and elec-

tric field are studied in both the equilateral triangular and symmetric linear TQD cases. In both cases, we find doublet-quartet transitions of ground-state spin configurations by varying either the dot size or interdot distance in the absence of external fields, which has not been reported in the literature on TQDs. Interestingly, we also observe anticrossings with large energy splittings between energy levels with the same spin state in the perpendicular magnetic-field dependence of the energy spectra in the absence of the SOC. These anticrossings, which have not been reported in the literature, originate from the equilateral triangular and symmetric linear TQD confinement potential, respectively. In contrast to the complex dependence on the perpendicular magnetic field, the energy spectra vary linearly with the parallel magnetic field due to the negligible orbital effect of parallel magnetic field. Additionally, in perpendicular/parallel magnetic-field dependence of energy levels, we find that all the intersections in equilateral triangular TQD cases become anticrossing due to the SOC whereas only part of them show anticrossing behaviors in symmetric linear TQD case. All these anticrossing behaviors are analyzed from the symmetry consideration. Moreover, we also find that energy levels and their charge configurations can be strongly affected by the in-plane electric field.

Acknowledgments

This work was supported by the National Basic Research Program of China under Grant No. 2012CB922002 and the Strategic Priority Research Program of the Chinese Academy of Sciences under Grant No. XDB01000000. One of the authors (YFR) would like to thank Y. Yin and M. Q. Weng for valuable discussions in numerical calculation.

Appendix A: ANTICROSSINGS DUE TO THE SOC IN TQDS

In this part, we show the detailed analysis about the anticrossing behavior due to the SOC in the magnetic field dependence of the energy spectra in both equilateral triangular and symmetric linear TQD cases. We focus on the perpendicular magnetic field case. To facilitate the understanding, we first review the anticrossing behavior in single QD limit.⁵⁹ In the absence of the SOC, the perpendicular magnetic-field dependence of the lowest few energy levels are plotted in Fig. 6. These energy levels are denoted by the good quantum numbers S_{tot} , S_z and L , and the intersections between them are simple crossings as mentioned previously.⁵⁹ With the inclusion of the SOC, part of these intersections (labelled by open squares in Fig. 6) are lifted to show anticrossing behavior. To understand this behavior, we span the Hilbert space by the three-electron eigenstates labelled by (L, S_{tot}, S_z) . It is noted that the Hilbert space is also

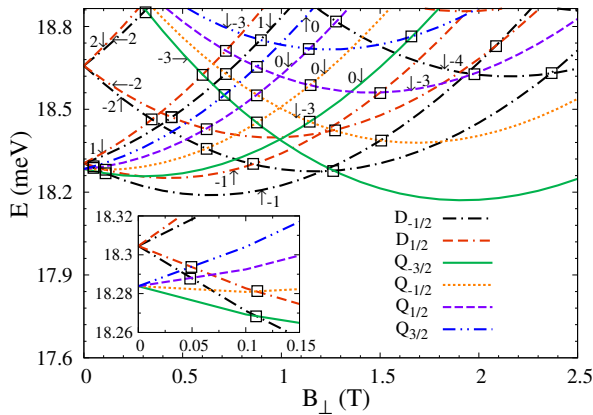


FIG. 6: (Color online) The lowest few energy levels *vs.* perpendicular magnetic field in single QDs. The total azimuthal angular momentum L of each energy level is labelled in the figure. Open squares denote the intersections which can become anticrossing due to the SOC. The inset enlarges the energy spectra in the vicinity of $B_{\perp} \sim 0$ T. $d_0 = 29$ nm.

spanned by these eigenstates in the following. As the eigenstate with (L, S_z) can be coupled with the one with $(L \pm 1, S_z \mp 1)$ or $(L \pm 1, S_z \pm 1)$ by the SOC [see Eq. (2)] according to the previous works,^{22,59} the Hilbert space can be divided into two independent parts spanned by the eigenstates with $L + S_z + 3/2$ being even or odd. The eigenstates in the same part can be coupled with each other by the SOC, which makes the intersections between

the energy levels in the same part become anticrossing.

With the increase of the interdot distance, we turn to study the equilateral triangular TQD case. As pointed out previously, the equilateral triangular TQD confinement potential can couple the eigenstates in single QDs with the same spin state and the difference of L being $3m$ (m integer). This indicates that two independent parts (i.e., $L + S_z + 3/2$ being even or odd) can be coupled by the TQD confinement potential. As a result, all the intersections in equilateral triangular TQD case can be lifted by the SOC.

As for the symmetric linear TQD case, the confinement potential can couple the eigenstates in single QDs with the same spin state and the difference of L being even. Thus, two independent parts (i.e., $L + S_z + 3/2$ being even or odd) are still independent, which is different from the equilateral triangular TQD case. As a result, only the intersections between the energy levels in the same part can show anticrossing behavior due to the SOC.

We also study the case of parallel magnetic field applied along x -axis. Similar to the case of perpendicular magnetic field, in single QD limit, the three-electron eigenstates can be divided into two independent parts according to $L + S_x + 3/2$ being either even or odd with the inclusion of the SOC.^{22,59} As for the TQD cases, we also find that all the intersections in equilateral triangular TQDs whereas only those between the energy levels in the same part (i.e., $L + S_x + 3/2$ being either even or odd) in symmetric linear TQDs can become anticrossing due to the SOC.

* wlf@mail.ustc.edu.cn

† mwwu@ustc.edu.cn

¹ D. Loss and D. P. DiVincenzo, Phys. Rev. A **57**, 120 (1998).

² S. M. Reimann and M. Manninen, Rev. Mod. Phys. **74**, 1283 (2002).

³ W. G. van der Wiel, S. De Franceschi, J. M. Elzerman, T. Fujisawa, S. Tarucha, and L. P. Kouwenhoven, Rev. Mod. Phys. **75**, 1 (2003).

⁴ R. Hanson, L. P. Kouwenhoven, J. R. Petta, S. Tarucha, and L. M. K. Vandersypen, Rev. Mod. Phys. **79**, 1217 (2007).

⁵ C.-Y. Hsieh, Y.-P. Shim, M. Korkusinski, and P. Hawrylak, Rep. Prog. Phys. **75**, 114501 (2012).

⁶ B. Urbaszek, X. Marie, T. Amand, O. Krebs, P. Voisin, P. Maletinsky, A. Högele, and A. Imamoglu, Rev. Mod. Phys. **85**, 79 (2013).

⁷ G. Burkard, D. Loss, and D. P. DiVincenzo, Phys. Rev. B **59**, 2070 (1999).

⁸ J. Levy, Phys. Rev. Lett. **89**, 147902 (2002).

⁹ J. M. Elzerman, R. Hanson, J. S. Greidanus, L. H. Willems van Beveren, S. De Franceschi, L. M. K. Vandersypen, S. Tarucha, and L. P. Kouwenhoven, Phys. Rev. B **67**, 161308(R) (2003).

¹⁰ J. L. Cheng, M. W. Wu, and C. Lü, Phys. Rev. B **69**,

115318 (2004).

¹¹ A. C. Johnson, J. R. Petta, J. M. Taylor, A. Yacoby, M. D. Lukin, C. M. Marcus, M. P. Hanson, and A. C. Gossard, Nature (London) **435**, 925 (2005).

¹² J. M. Taylor, H. A. Engel, W. Dür, A. Yacoby, C. M. Marcus, P. Zoller, and M. D. Lukin, Nat. Phys. **1**, 177 (2005).

¹³ J. R. Petta, A. C. Johnson, J. M. Taylor, E. A. Laird, A. Yacoby, M. D. Lukin, C. M. Marcus, M. P. Hanson, and A. C. Gossard, Science **309**, 2180 (2005).

¹⁴ C. P. García, V. Pellegrini, A. Pinczuk, M. Rontani, G. Goldoni, E. Molinari, B. S. Dennis, L. N. Pfeiffer, and K. W. West, Phys. Rev. Lett. **95**, 266806 (2005).

¹⁵ F. H. L. Koppens, C. Buizert, K. J. Tielrooij, I. T. Vink, K. C. Nowack, T. Meunier, L. P. Kouwenhoven, and L. M. K. Vandersypen, Nature (London) **442**, 766 (2006).

¹⁶ K. Shen and M. W. Wu, Phys. Rev. B **76**, 235313 (2007).

¹⁷ J. M. Taylor, J. R. Petta, A. C. Johnson, A. Yacoby, C. M. Marcus, and M. D. Lukin, Phys. Rev. B **76**, 035315 (2007).

¹⁸ J. H. Jiang, Y. Y. Wang, and M. W. Wu, Phys. Rev. B **77**, 035323 (2008).

¹⁹ F. H. L. Koppens, K. C. Nowack, and L. M. K. Vandersypen, Phys. Rev. Lett. **100**, 236802 (2008).

²⁰ S. Foletti, H. Bluhm, D. Mahalu, V. Umansky, and A.

- Yacoby, *Nat. Phys.* **5**, 903 (2009).
- 21 D. Culcer, L. Cywiński, Q. Li, X. Hu, and S. Das Sarma, *Phys. Rev. B* **80**, 205302 (2009).
- 22 L. Wang, K. Shen, B. Y. Sun, and M. W. Wu, *Phys. Rev. B* **81**, 235326 (2010).
- 23 M. Xiao, M. G. House, and H. W. Jiang, *Appl. Phys. Lett.* **97**, 032103 (2010).
- 24 M. Xiao, M. G. House, and H. W. Jiang, *Phys. Rev. Lett.* **104**, 096801 (2010).
- 25 D. Culcer, L. Cywiński, Q. Z. Li, X. D. Hu, and S. Das Sarma, *Phys. Rev. B* **82**, 155312 (2010).
- 26 F. Baruffa, P. Stano, and J. Fabian, *Phys. Rev. B* **82**, 045311 (2010).
- 27 M. G. Borselli, R. S. Ross, A. A. Kiselev, E. T. Croke, K. S. Holabird, P. W. Deelman, L. D. Warren, I. Alvarado-Rodriguez, I. Milosavljevic, F. C. Ku, W. S. Wong, A. E. Schmitz, M. Sokolich, M. F. Gyure, and A. T. Hunter, *Appl. Phys. Lett.* **98**, 123118 (2011).
- 28 M. Raith, P. Stano, and J. Fabian, *Phys. Rev. B* **83**, 195318 (2011).
- 29 L. Wang and M. W. Wu, *J. Appl. Phys.* **110**, 043716 (2011).
- 30 M. Raith, P. Stano, and J. Fabian, *Phys. Rev. B* **86**, 205321 (2012).
- 31 D. P. DiVincenzo, D. Bacon, J. Kempe, G. Burkard, and K. B. Whaley, *Nature (London)* **408**, 339 (2000).
- 32 E. A. Laird, J. M. Taylor, D. P. DiVincenzo, C. M. Marcus, M. P. Hanson, and A. C. Gossard, *Phys. Rev. B* **82**, 075403 (2010).
- 33 S. Mehl and D. P. DiVincenzo, *Phys. Rev. B* **87**, 195309 (2013).
- 34 J. M. Taylor, V. Srinivasa, and J. Medford, arXiv:1304.3407v2.
- 35 I. P. Gimenez, C.-Y. Hsieh, M. Korkusinski, and P. Hawrylak, *Phys. Rev. B* **79**, 205311 (2009).
- 36 C.-Y. Hsieh, A. Rene, and P. Hawrylak, *Phys. Rev. B* **86**, 115312 (2012).
- 37 A. Acín, D. Bruß, M. Lewenstein, and A. Sanpera, *Phys. Rev. Lett.* **87**, 040401 (2001).
- 38 C. H. Bennett, G. Brassard, C. Crépeau, R. Jozsa, A. Peres, and W. K. Wootters, *Phys. Rev. Lett.* **70**, 1895 (1993).
- 39 A. M. Steane, *Phys. Rev. Lett.* **77**, 793 (1996).
- 40 C. F. Roos, M. Riebe, H. Häffner, W. Hänsel, J. Benhelm, G. P. T. Lancaster, C. Becher, F. Schmidt-Kaler, and R. Blatt, *Science* **304**, 1478 (2004).
- 41 A. Sharma and P. Hawrylak, *Phys. Rev. B* **83**, 125311 (2011).
- 42 L. Gaudreau, S. A. Studenikin, A. S. Sachrajda, P. Zawadzki, A. Kam, J. Lapointe, M. Korkusinski, and P. Hawrylak, *Phys. Rev. Lett.* **97**, 036807 (2006).
- 43 G. Yamahata, Y. Tsuchiya, H. Mizuta, K. Uchida, and S. Oda, *Solid State Electronics* **53**, 779 (2009).
- 44 G. Granger, L. Gaudreau, A. Kam, M. Pioro-Ladrière, S. A. Studenikin, Z. R. Wasilewski, P. Zawadzki, and A. S. Sachrajda, *Phys. Rev. B* **82**, 075304 (2010).
- 45 F. R. Braakman, P. Barthelemy, C. Reichl, W. Wegscheider, and L. M. K. Vandersypen, *Appl. Phys. Lett.* **102**, 112110 (2013).
- 46 M. Pierre, R. Wacquez, B. Roche, X. Jehl, M. Sanquer, M. Vinet, E. Prati, M. Belli, and M. Fanciulli, *Appl. Phys. Lett.* **95**, 242107 (2009).
- 47 S. Amaha, T. Hatano, T. Kubo, S. Teraoka, Y. Tokura, S. Tarucha, and D. G. Austing, *Appl. Phys. Lett.* **94**, 092103 (2009).
- 48 H. Pan, M. G. House, X. Hao, and H. W. Jiang, *Appl. Phys. Lett.* **100**, 263109 (2012).
- 49 L. Gaudreau, G. Granger, A. Kam, G. C. Aers, S. A. Studenikin, P. Zawadzki, M. Pioro-Ladrière, Z. R. Wasilewski, and A. S. Sachrajda, *Nat. Phys.* **8**, 54 (2012).
- 50 J. Medford, J. Beil, J. M. Taylor, S. D. Bartlett, A. C. Doherty, E. I. Rashba, D. P. DiVincenzo, H. Lu, A. C. Gossard, and C. M. Marcus, arXiv:1302.1933.
- 51 V. W. Scarola, K. Park, and S. Das Sarma, *Phys. Rev. Lett.* **93**, 120503 (2004).
- 52 P. Hawrylak and M. Korkusinski, *Solid State Commun.* **136**, 508 (2005).
- 53 V. W. Scarola and S. Das Sarma, *Phys. Rev. A* **71**, 032340 (2005).
- 54 M. Korkusinski, I. P. Gimenez, P. Hawrylak, L. Gaudreau, S. A. Studenikin, and A. S. Sachrajda, *Phys. Rev. B* **75**, 115301 (2007).
- 55 I. P. Gimenez, M. Korkusinski, and P. Hawrylak, *Phys. Rev. B* **76**, 075336 (2007).
- 56 F. Delgado, Y.-P. Shim, M. Korkusinski, and P. Hawrylak, *Phys. Rev. B* **76**, 115332 (2007).
- 57 B. R. Bulka, T. Kostyrko, and J. Łuczak, *Phys. Rev. B* **83**, 085301 (2011).
- 58 C.-Y. Hsieh, Y.-P. Shim, and P. Hawrylak, *Phys. Rev. B* **85**, 085309 (2012).
- 59 Z. Liu, L. Wang, and K. Shen, *Phys. Rev. B* **85**, 045311 (2012).
- 60 G. Dresselhaus, *Phys. Rev.* **100**, 580 (1955).
- 61 E. I. Rashba, *Fiz. Tivverd. Tela (Leningrad)* **2**, 1224 (1960).
- 62 L. Vervoort, R. Ferreira, and P. Voisin, *Phys. Rev. B* **56**, R12744 (1997).
- 63 C. Tahan and R. Joynt, *Phys. Rev. B* **71**, 075315 (2005).
- 64 M. O. Nestoklon, E. L. Ivchenko, J. M. Jancu, and P. Voisin, *Phys. Rev. B* **77**, 155328 (2008).
- 65 Q. Li, L. Cywiński, D. Culcer, X. Hu, and S. Das Sarma, *Phys. Rev. B* **81**, 085313 (2010).
- 66 J. J. L. Morton, D. R. McCamey, M. A. Eriksson, and S. A. Lyon, *Nature* **479**, 345 (2011).
- 67 R. Vrijen, E. Yablonoitch, K. Wang, H. W. Jiang, A. Balandin, V. Roychowdhury, T. Mor, and D. DiVincenzo, *Phys. Rev. A* **62**, 012306 (2000).
- 68 M. Friesen, S. Chutia, C. Tahan, and S. N. Coppersmith, *Phys. Rev. B* **75**, 115318 (2007).
- 69 T. Ando, A. B. Fowler, and F. Stern, *Rev. Mod. Phys.* **54**, 437 (1982).
- 70 S. Goswami, K. A. Slinker, M. Friesen, L. M. McGuire, J. L. Truitt, C. Tahan, L. J. Klein, J. O. Chu, P. M. Mooney, D. W. van der Weide, R. Joynt, S. N. Coppersmith, and M. A. Eriksson, *Nat. Phys.* **3**, 41 (2007).
- 71 V. Fock, *Z. Phys.* **47**, 446 (1928).
- 72 C. G. Darwin, *Proc. Cambridge Philos. Soc.* **27**, 86 (1931).
- 73 C. F. O. Graeff, M. S. Brandt, M. Stutzmann, M. Holzmann, G. Abstreiter, and F. Schäffler, *Phys. Rev. B* **59**, 13242 (1999).
- 74 W. Gerlach and O. Stern, *Ann. Phys.* **74**, 673 (1924).
- 75 P. Stano and J. Fabian, *Phys. Rev. B* **72**, 155410 (2005).
- 76 Y. Hada and M. Eto, *Phys. Rev. B* **68**, 155322 (2003).
- 77 S. Capstick and N. Isgur, *Phys. Rev. D* **34**, 2809 (1986).
- 78 W. Greiner and B. Müller, *Quantum Mechanics: Symmetries* (Springer, New York, 1994).
- 79 For quartet states, the total spin $S_{\text{tot}} = 3/2$ and its component parallel to the external magnetic field along the $z(x)$ -direction is $S_{z(x)} = \pm 1/2, \pm 3/2$. As for the doublet

states, $S_{\text{tot}} = 1/2$ and $S_{z(x)} = \pm 1/2$.

- ⁸⁰ J. J. Sakurai, *Modern Quantum Mechanics* (Addison-Wesley, Reading, 1994).
- ⁸¹ J.-M. Richard, arXiv:1205.4326v2.
- ⁸² The matrix elements of Coulomb interaction are obtained according to Ref. 26 reported by Baruffa *et al.*.
- ⁸³ R. N. Dexter, B. Lax, A. F. Kip, and G. Dresselhaus, *Phys. Rev.* **96**, 222 (1954).
- ⁸⁴ G. F. Koster, J. O. Dimmock, R. G. Wheeler, and H. Statz, *Properties of the Thirty-Two Point Groups* (MIT Press,

Cambridge, 1963).

- ⁸⁵ n_i can be calculated by $n_i = 3 \int_{\Omega_i} d\mathbf{r}_1 \iint d\mathbf{r}_2 d\mathbf{r}_3 |\Psi(\mathbf{r}_1, \mathbf{r}_2, \mathbf{r}_3)|^2$, where Ψ is the wavefunction of three-electron eigenstate. The region of integration for the first integral is Ω_i in which the position is nearest to the center of the i th QD, whereas the region is the whole two dimensional real space for the second and third ones.